MECH-139

MIXED MODE FRACTURE MECHANICS OF INTERFACES

John W. Hutchinson

Division of Applied Sciences
HARVARD UNIVERSITY
Cambridge, Massachusetts 02138

February 1989

Published in:
Metal-Ceramic Interfaces, Acta-Scripta Metallurgica Proceedings Series, Volume 4, edited by M. Rühle, A. G. Evans, M. F. Ashby and J. P. Hirth, Pergamon Press, 1990, pp. 295-306.

MIXED MODE FRACTURE MECHANICS OF INTERFACES

John W. Hutchinson
Division of Applied Sciences
Harvard University
Cambridge, MA 02138

Introduction

This paper reviews some recent developments in the mechanics of fracture of interfaces between elastic materials. The review draws heavily on the recent work of the author and his collaborators at Harvard and the University of California, Santa Barbara.

Due to asymmetry in loading and elastic properties across the interface, many interfacial fracture problems are inherently mixed mode. In mixed mode, both normal and shear stresses act across the interface ahead of the tip of the interfacial crack, and both opening and shearing displacements occur on the crack faces behind the tip. Thus interfacial fracture in two-dimensional geometries involves mode 1 (opening) and mode 2 (shearing) stress intensity factors, and one must allow for a toughness characterization which, in general, is a function of the relative amounts of mode 1 and mode 2. This is one of the main differences between interfacial fracture mechanics and fracture mechanics for isotropic homogeneous materials in which mode 1 toughness receives predominant emphasis.

This review starts off with a discussion of universal crack tip fields at an interface between dissimilar isotropic elastic solids. Then, examples are given which illustrate the extent to which loading and moduli differences influence conditions at the tip. Some mixed mode toughness data are presented and related to preliminary micromechanics modeling. Decohesion of coatings and thin films is discussed within the context of interfacial fracture, and some first results of an analysis of the cut test are reported wherein decohesion is induced by a straight cut through a residually stressed coating. The final example deals with the deflection of a crack into an interface.

Crack Tip Fields

With the interface on the x_1-axis, let E_1, μ_1 and ν_1 be the Young's modulus, shear modulus and Poisson's ratio of material 1 lying above the interface ($x_2 > 0$) with similar quantities, E_2, μ_2 and ν_2, for material 2 lying below the interface. For plane problems with traction boundary conditions, only two nondimensional combinations of the four independent material moduli parameters enter into any solution (1). For plane strain the moduli mismatch parameters of Dundurs are

$$\alpha = \frac{\bar{E}_1 - \bar{E}_2}{\bar{E}_1 + \bar{E}_2} \quad \text{and} \quad 2\beta = \frac{\mu_1(1-2\nu_2) - \mu_2(1-2\nu_1)}{\mu_1(1-\nu_2) + \mu_2(1-\nu_1)} \qquad [1]$$

where $\bar{E} = E/(1-\nu^2)$ is the plane strain tensile modulus. Note that α and β both vanish when dissimilarity between the elastic properties of the materials is absent, and α and β change signs when the materials are switched.

For each material pair, a universal singular crack tip field exists at the crack tip according to linear elasticity theory for a traction-free line crack. For the plane problems, the normal and shear stresses of the singular field acting on the interface a distance r ahead of the tip can be written in the compact "complex" form

$$\sigma_{22} + i\sigma_{12} = \frac{(K_1 + iK_2)r^{i\varepsilon}}{\sqrt{2\pi r}} \qquad [2]$$

where $i \equiv \sqrt{-1}$ and the oscillation index ε depends on β according to

$$\varepsilon = \frac{1}{2\pi} \ln\left(\frac{1-\beta}{1+\beta}\right) \qquad [3]$$

In plane strain the crack face displacements a distance r behind the tip, $\delta_i = u_i(-r,0^+) - u_i(-r,0^-)$, are given by

$$\delta_2 + i\delta_1 = \frac{4}{\sqrt{2\pi}} \frac{(1/\bar{E}_1+1/\bar{E}_2)}{(1+2i\varepsilon)\cosh(\pi\varepsilon)} (K_1+iK_2)\sqrt{r}\ r^{i\varepsilon} \qquad [4]$$

The amplitude factors, K_1 and K_2, depend linearly on the applied loads and on the details of the full geometry of the body, as will be illustrated below. These stress intensity factors are defined to be consistent with corresponding stress intensity factors for cracks in homogeneous problems (2). The energy release rate per unit length of extension of the crack in the interface is related to the stress intensity factors by (for plane strain)

$$\mathcal{G} = \frac{[1/\bar{E}_1+1/\bar{E}_2]}{2\cosh^2\pi\varepsilon} (K_1^2+K_2^2) \qquad [5]$$

which is the generalization of Irwin's famous result for a homogeneous isotropic material.

When $\varepsilon \neq 0$, the relative proportion of normal and shear stresses on the interface in the singular field varies slowly according to $r^{i\varepsilon} \equiv \cos(\varepsilon \ln r) + i \sin(\varepsilon \ln r)$, and this feature complicates the implementation of interfacial mechanics in several respects. When $\varepsilon \neq 0$, the traction-free line crack solution is not fully consistent since the solution [4] implies that the crack faces interpenetrate behind the tip. Although seemingly troublesome, this inconsistency will usually be inconsequential since the distance of the contact region behind the tip is generally exceedingly small compared to the zone of nonlinear deformation or fracture processes. More problematic is the fact that K_1 and K_2 cannot be interpreted in a straightforward way as mode 1 and mode 2 intensity factors directly linked to normal and shear stresses. Moreover, the combination K_1+iK_2 has dimensional units of stress σ and length L in the form $\sigma\sqrt{L}L^{-i\varepsilon}$. A peculiar consequence of the dimensional form is that the relative proportion of a critical combination (K_1, K_2) changes when units are changed (2).

The features mentioned above have stood as conceptual stumbling blocks in the development of interfacial fracture mechanics even though there is no compelling evidence to date to suggest that "ε-effects" are important. For many pairs of materials of interest one finds that ε is very small, e.g. less than a few hundredths in magnitude, even when α is substantial corresponding to ratios of the $\bar{E}$'s of 4 or 5 or more. An extensive tabulation of (α,β) pairs is presented in (3). At this stage in the development of interfacial fracture mechanics it is likely that the role of ε is far less important than other problems and issues, including even the simplification of elastic isotropy. Thus, various proposals have been put forth for ignoring ε. A consistent approach proposed in (4,5) is to systematically take $\beta = 0$ (and thus $\varepsilon = 0$), both in the determination of critical toughness data from test specimens and in subsequent application of such data to predict fracture. In other words, for a given material pair one contemplates another pair with slightly perturbed elastic moduli leading to $\beta = 0$ for the purpose of analyzing specimens and making applications.

With $\varepsilon = 0$, $r^{i\varepsilon} = 1$ in [2] and [4], and then K_1 and K_2 have conventional interpretations as mode 1 and mode 2 stress intensity factors measuring the singularity of normal and shear stresses, respectively, on the interface ahead of the tip. At various points throughout this review the assumption is that $\varepsilon = 0$ will be invoked in the above spirit. Recent work (6-9) has dealt with crack tip fields for an interface crack lying on an interface between dissimilar anisotropic elastic solids, and general restrictions on the moduli leading to nonoscillatory fields and conventional stress intensity factors have been identified.

Some Basic Solutions

A number of relatively simple exact solutions were given in the original papers on interface cracks from the 1960's (see (2) for a listing of these references). For a crack of length $2a$ lying on the interface between two semi-infinite blocks subject to remote stress (see Fig. 1a), the stress intensity factors of the right-hand tip are

$$K_1 + iK_2 = (\sigma_{22}^{\infty}+i\sigma_{12}^{\infty})(1+2i\epsilon)(2a)^{-i\epsilon}\sqrt{\pi a} \qquad [6]$$

This solution does not depend on α, and perhaps it is partly for this reason that so much emphasis was placed on the role of ϵ in the beginning development of the subject. When $\epsilon = 0$ (recalling that the magnitude of ϵ is often only a few hundredths or less), [6] reduces to the classical result for the mode I and mode II stress intensity factors for a crack in a homogeneous, isotropic elastic solid.

Next, consider the semi-infinite interface crack between two infinite elastic layers shown in Fig. 1b and subject to the general loading indicated. This problem has been solved completely in (10). An exact expression for the energy release rate $\mathcal{G}$ can be obtained in closed form, which by [5] gives the magnitude of K_1+iK_2. Integral equation methods have been used to obtain the relative proportion of K_2 to K_1. Complete details of the solution are given in (10); the form of the solution is

$$K_1 + iK_2 = \left[c_1 P h^{-1/2}+c_2 M h^{-3/2}\right] h^{-i\epsilon} \qquad [7]$$

where P (load per unit thickness) and M (moment per unit thickness) are linear combinations of the P_i's and M_i's, and c_1 and c_2 are dimensionless complex numbers depending on α, β and h/H. Application of this general result will be made to two problems in the next section.

Another complete solution is available for sandwich geometries wherein a thin layer of material 2 is sandwiched between two planar bodies of material 1 with an interface crack lying between the thin layer and the upper block. Let K_I and K_{II} be the conventional mode I and mode II stress intensity factors for the homogeneous body of material 1 in the absence of the middle layer. If the thickness of the sandwich layer h is very small compared to the crack length and to all other relevant in-plane length quantities, a universal asymptotic relation exists between the interface intensity factors, K_1 and K_2, and the stress intensity factors, K_I and K_{II}, for the homogeneous problem. The factors K_I and K_{II}, can be thought of as applied, or remote, stress intensities for the semi-infinite crack problem depicted in Fig. 1c. The asymptotic relation between the interface stress intensities and the applied stress intensities is

$$K_1 + iK_2 = \sqrt{\frac{1-\alpha}{1-\beta^2}}\,(K_I+iK_{II})h^{-i\epsilon}e^{i\omega(\alpha,\beta)} \qquad [8]$$

where the real function $\omega(\alpha,\beta)$ is tabulated in (5). Thus, for example, if stress intensity factors K_I and K_{II} are known for a test specimen with homogeneous moduli, [8] is the universal relation giving the interface intensity factors for the corresponding sandwich specimens. The energy release rate $\mathcal{G}$ in this asymptotic problem is equal to the applied energy release rate $(1-\nu_1^2)(K_I^2+K_{II}^2)/E_1$, as is readily seen from [8] with [5]. The β-dependence of ω is weak; $\omega(\alpha,0)$ is plotted in Fig. 2. For $\beta = 0$, [8] reduces to

$$K_1 + iK_2 = \sqrt{1-\alpha}\,(K_I+iK_{II})e^{i\omega(\alpha,0)} \qquad [9]$$

so that ω represents the shift in "phase" of the interface intensity factors relative to the applied intensity factors, i.e.

$$\tan^{-1}(K_2/K_1) = \tan^{-1}(K_{II}/K_I) + \omega \qquad [10]$$

From Fig. 2 it is seen that this shift, which is due exclusively to the moduli mismatch, ranges between 5° and -15°, depending on α. For most material pairs this will not be a large effect.

Some Examples

The examples shown in Fig. 3 have been chosen to illustrate the range of mixed mode conditions which can arise in applications of interfacial fracture mechanics. For discussion purposes (as well as in actual implementation in many cases), it will be assumed that $\beta = 0$. Let

$$\psi = \tan^{-1}(K_2/K_1) \qquad [11]$$

measure the "phase" of the stress intensity factors so that $\psi = 0°$ corresponds to pure mode 1 and $\psi = 90°$ corresponds to pure mode 2.

The *double cantilever specimen* in Fig. 3a is a special case of the two-layer problem in Fig. 1b. Specializing the results of (10) to this specific loading and geometry gives (with $\beta = 0$)

$$K_1 + iK_2 = 2\sqrt{3}\ Mh^{-3/2}e^{i\psi} \qquad [12]$$

where ψ is plotted as a function of α in Fig. 4. The symmetry of the geometry and the loading dictates that the specimen must be pure mode 1 when there is continuity of moduli across the interface (i.e. when $\alpha = 0$). When $\alpha \neq 0$, the asymmetry due to the moduli mismatch induces a mode 2 component which can be appreciable when, for example, $\alpha = \pm .5$, corresponding to $\bar{E}_1/\bar{E}_2 = 3$ or $1/3$.

Figure 3b depicts a *thin film or coating* of material 1 with residual biaxial tensile stress σ attached to a thick substrate of material 2. The film is decohering along the interface driven by the residual stress. When the decohesion crack length is long compared to the film thickness, conditions at the tip approach a steady state which is independent of crack length. For the limit when the film thickness h is very small compared to the substrate thickness H (i.e. $h/H \to 0$), the steady state energy release rate is

$$\mathcal{G} = \frac{1}{2}(1-\nu_1^2)\sigma^2 h/E_1 \qquad [13]$$

The interface intensity factors can be obtained by specializing the results in (10). When $\beta = 0$,

$$K_1 + iK_2 = \sqrt{\frac{1-\alpha}{2}}\ \sigma h^{1/2}e^{i\psi} \qquad [14]$$

where ψ is plotted in Fig. 5. It is noted that decohesion cracking is inherently mixed mode with ψ ranging from 45° to 70°, depending on α.

The *four-point bend specimen* in Fig. 3c has been analyzed and used for measuring interfacial toughness for several material combinations (11, 12). The specimen has the advantage that the crack tip is in steady-state condition when the crack is long compared to the thickness but still between the inner loading points. The results for the two-layer problem in Fig. 1b can be used to analyze the specimen when the crack is advancing under steady-state conditions. The analysis, which is given in (10), is highly accurate when the total thickness of the specimen is small compared to the distance between the loading points. Over a fairly wide range of α and h/H the analysis predicts $\psi \cong 45°$. Thus, this specimen measures mixed mode toughness under conditions when K_1 and K_2 are approximately equal.

The final example considered is the *fiber pull-out problem* depicted in Fig. 3d. This problem is of considerable interest in connection with the role of fibers in bridging matrix cracks in brittle matrix composites. For the fiber to perform effectively it is essential that it debond from the matrix some distance away from the main matrix crack. This debonding permits fiber pull-out and a consequent toughening contribution from the fiber. There are a variety of conditions under which it is important to understand the fiber debonding process, and many

of these remain to be analyzed. One numerical analysis (13), applicable when there is a residual tensile stress acting across the fiber/matrix interface prior to debonding, predicts that the interface debonding crack is heavily mode 2, as might be expected from the loading and geometry, with $\psi \equiv 75°$.

Interfacial Toughness

The examples of Fig. 3 are intended to drive home the point that interfacial fracture conditions can range from mode 1 to mode 2 and are often decidedly mixed. The specification of interface toughness when $\varepsilon \neq 0$ has been discussed in (2). As noted earlier, the specification is simplified when $\varepsilon = 0$ since K_1 and K_2 then have straightforward interpretations as mode 1 and mode 2 intensity factors. Here we will confine the discussion to material pairs for which $\varepsilon = 0$, either exactly or by approximation.

In general one must expect that the toughness of the interface (i.e. the critical value of $\mathcal{G}$ associated with crack advance in the interface) is a function of the combination of K_1 and K_2 governing the crack tip stresses. That is, the specification of interface toughness requires that $\mathcal{G}_c$ be known as a function of $\psi = \tan^{-1}(K_2/K_1)$. The attainment of conditions for crack advance in the interface is stated formally as

$$\mathcal{G} = \mathcal{G}_c(\psi) \qquad [15]$$

where $\mathcal{G}$ is given in terms of K_1 and K_2 by [5]. It may be that an "ideally brittle" interface will have a toughness $\mathcal{G}_c$ which is independent of ψ and equal to the energy needed to create the two free surfaces. No mixed mode toughness data exists yet to show that "ideally brittle" interfaces actually exist. In fact, very little experimental toughness data exists which systematically spans a range of ψ. One recent set of data for $\mathcal{G}_c(\psi)$, shown in Fig. 6, was generated in (12) for an epoxy bonded to glass. The experimental data was obtained using a variety of specimens such as those in Fig. 3 to span the range of ψ from pure mode 1 to $\psi \equiv 75°$. For this material pair and for the conditions under which the surfaces were bonded, the toughness is clearly a strong function of the combination of modes at the crack tip.

A first attempt at a micromechanics model of interfacial toughness as it is influenced by non-planarity of the fractured interface was given in (14). The idealized situation envisioned is depicted in Fig. 7a. Due either to the intrinsic faceting of the interface in the bonded state (15) or to roughness generated by the fracture process itself, the fracture surfaces are taken to have facets of height w and spacing l. Within the vicinity of the crack tip where the crack opening displacement, δ_2, is less than w, the facets on opposite faces contact one another and tend to shield the tip from the full effect of K_2 when K_2 is not zero. The analysis in (14), which neglects any dissimilarity in moduli, derives an estimate for $\mathcal{G}_c(\psi)$ based on the criterion that the shielded energy release rate at the tip equals the "intrinsic" toughness $\mathcal{G}_c^0$, which can also be identified with the pure mode 1 toughness.

The effective interface toughness depends on a single nondimensional material/roughness parameter R which is predominantly dependent on

$$\frac{Ew^2}{l\mathcal{G}_c^0} \qquad [16]$$

(A full specification of R is given in (14).) Plots of the normalized toughness increase as a function of ψ for different levels of interface roughness R are shown in Fig. 7b. Included in Fig. 7b is the experimental data of Fig. 6 from (12) for the epoxy/glass interface. The measured roughness of the fractured interface is in approximate agreement with the roughness level $R \equiv 1$ indicated by the model predictions in Fig. 7b (12). In the limiting result for $\mathcal{G}_c(\psi)$ when $R \to \infty$, K_2 has no influence on the energy release rate at the tip, as the model in Fig. 7a would suggest. Thus, for all ψ the energy release rate at the tip is $(1-\nu^2)K_1^2/E$ and, consequently,

$$\mathcal{G}_c(\psi) = \mathcal{G}_c^0[1 + \tan^2\psi] \qquad [17]$$

Clearly the epoxy/glass interface behaves more like a highly rough interface than an ideally brittle one.

Other microscopic processes can be expected to influence the mixed-mode toughness. These include friction and plasticity, either dislocation emission at the tip or more extensive zones of high dislocation density.

Decohesion of Thin Films

A necessary condition for a thin film under residual biaxial tension σ to undergo extensive decohesion can be inferred from the results [13] and [14] for the plane strain problem in Fig. 3b. When the substrate is thick compared to the film ($h/H \to 0$) the critical stress for steady-state, two-dimensional cracking is

$$\sigma_c = \sqrt{\frac{2\mathcal{G}_c(\psi)E_1}{(1-\nu_1^2)h}} \qquad [18]$$

where ψ is obtained from Fig. 5. Decohesion of regions whose extent is large compared to the thickness will only occur if $\sigma > \sigma_c$. In the *cut test* a straight cut, many times h in length, is made through the film. If $\sigma > \sigma_c$, a region of decohesion spreads from the cut. The equilibrium shape of the decohered region is governed by the condition that the crack driving force, $\mathcal{G}$, at every point along the edge of the decohesion just attains the condition for further decohesion.

Because both normal and shear stresses act along the decohesion boundary, the interface crack front is fully mixed mode with mode 3 present as well as modes 1 and 2. The energy release rate under the three modes is (with $\beta = 0$)

$$\mathcal{G} = \frac{1}{2}\left(\frac{1}{\bar{E}_1} + \frac{1}{\bar{E}_2}\right)\left(K_1^2 + K_2^2\right) + \frac{1}{4}\left(\frac{1}{\mu_1} + \frac{1}{\mu_2}\right)K_3^2 \qquad [19]$$

Along the decohesion boundary in the cut test the nature of the local stressing is such that the relative proportion of K_2 to K_1 is fixed with $\psi = \tan^{-1}(K_2/K_1)$ given by Fig. 5. Thus the shape of the decohered region can not be used to discriminate the role of K_2 in the decohesion criterion. However, the shape of the boundary is sensitive to how K_3 influences the decohesion criterion. An extensive study of this shape dependence is given in (16). Here we will report the shapes of the decohesion boundary for two limiting decohesion criteria suggested in the previous section: (i) based on an ideally brittle interface with $\mathcal{G} = \mathcal{G}_c^0$ where $\mathcal{G}_c^0$ is mode-independent, and (ii) based on a critical value of K_1, independent of K_2 and K_3.

The shapes of the decohesion boundary based on the criterion $\mathcal{G} = \mathcal{G}_c^0$ are shown in Fig. 8a. The critical stress parameter σ_c is given by [18] with $\mathcal{G}_c(\psi) \equiv \mathcal{G}_c^0$. Once the decohesion criterion has been specified, the shape and extent of the decohesion depends only on σ/σ_c and the Poisson's ratio of the film ν_1. The shapes corresponding to the criterion $K_1 = K_1^c$, independent of K_2 and K_3, are shown in Fig. 8b. The critical stress is still given by [18], but now

$$\mathcal{G}_c(\psi) = \frac{1}{2}\left(\frac{1}{\bar{E}_1} + \frac{1}{\bar{E}_2}\right)\left(K_1^c\right)^2 \frac{1}{\cos^2\psi} \qquad [20]$$

where ψ is obtained from Fig. 5. The most notable difference between the two families of shapes is that the decohesion boundary stands off the end of the cut when the criterion $\mathcal{G} = \mathcal{G}_c^0$ holds but remains attached when the criterion is based on a critical value of K_1. Observation of the cut test for a polyamide/glass system indicates

that the decohesion boundary remains attached for this systems (16). Furthermore, by considering a range of criteria, involving varying proportions of the mode 3 contribution, and the corresponding shape dependence, it is possible to draw some conclusions about the quantitative role of mode 3 on the decohesion criterion (16).

Crack Deflection Versus Penetration at an Interface

Whether an interface crack propagates within the interface or kinks out of the interface into one of the adjoining materials depends in an essential way on the combination of modes acting at the tip of the crack (4). It is also true that the tendency of a crack approaching an interface to deflect into the interface, as opposed to penetrating through the interface, depends essentially on mixed mode considerations, as will now be illustrated using an example from (17).

Consider the crack in Fig. 9a impinging at a right angle to the interface and assume the loading is symmetric with respect to the crack. Now consider two competing trajectories of crack advance: penetration of the interface in Fig. 9b, and deflection into the interface in Fig. 9c. In each case, the energy release rate, $\mathcal{G}$, is proportional to $a^{1-2\lambda}$, where a is the putative crack length and λ is the exponent of the stress singularitiy of ($\sigma \sim r^{-\lambda}$) of the problem in Fig. 9a. The ratio, $\mathcal{G}_d/\mathcal{G}_p$, is independent of a when a is small compared to the length of the main crack. Thus, the *relative* tendency of the crack to deflect or penetrate can be assessed using this ratio. Figure 10a shows this ratio as a function of α when $\beta = 0$. The proportion of mode 2 to mode 1 for the deflected crack is shown in Fig. 10b. (The penetrating crack is in pure mode 1.)

The condition (a necessary condition) for the crack to be deflected into the interface, rather than to penetrate it, is

$$\frac{\mathcal{G}_c(\psi)}{\mathcal{G}_c^{(1)}} < \frac{\mathcal{G}_d}{\mathcal{G}_p} \qquad [21]$$

where $\mathcal{G}_c(\psi)$ is the toughness of the interface at the relevant combination of modes and $\mathcal{G}_c^{(1)}$ is the mode 1 toughness of material 1 across the interface. When the elastic mismatch is not large ($\alpha \equiv 0$) , the condition requires that the interface toughness be less than about 1/4 the toughness of material 1, where the interface toughness is that associated with $\psi \equiv 45°$. Deflection as a symmetric doubly-deflected crack has also been considered in (17). Generally, the singly-deflected crack of Fig. 9c is the controlling case, but this conclusion depends somewhat on how strongly $\mathcal{G}_c(\psi)$ depends on ψ since the ψ-values differ for the two cases.

Acknowledgements

This work was supported in part by DARPA University Research Initiative (Subagreement P.O. #VB38639-0 with the University of California, Santa Barbara, ONR Prime Contract N00014-86-K-0753), by the National Science Foundation under Grant MSM-88-12779, and by the Division of Applied Sciences, Harvard University.

References

1. J. Dundurs, J. Appl. Mech., 36, p. 650 (1969)
2. J. R. Rice, J. Appl. Mech., 55, p. 98 (1988).
3. T. Suga, G. Elssner and S. Schmauder, J. Composite Materials, p. 917 (1988).
4. M-Y. He and J. W. Hutchinson, "Kinking of a crack out of an interface", to be published in J. Appl. Mech.
5. Z. Suo and J. W. Hutchinson, "On sandwich test specimens for measuring interface crack toughness", to be published in Materials Science and Engineering.
6. J. L. Bassani and J. Qu, "Finite crack on bimaterial and bicrystal interfaces", to be published in J. Mech. Phys. Solids.

7. T. C. T. Ting, Int. J. Solids Struct., 22, p. 965 (1986).
8. V. K. Tewary, R. H. Wagoner and J. P. Hirth, J. Mater. Res. 4, p. 124 (1989).
9. Z. Suo, "Singularities, interfaces and cracks in dissimilar anisotropic media", to be published.
10. Z. Suo and J. W. Hutchinson, "Interface crack between two elastic layers", to be published in Int. J. of Fracture.
11. P. G. Charalambides, J. Lund and A. G. Evans, "A test specimen for determining the fracture resistance of bimaterial interfaces", to be published in J. Appl. Mech.
12. H. C. Cao and A. G. Evans, "An experimental study of the fracture resistance of bimaterial interfaces", to be published in Mech. of Maters.
13. P. G. Charalambides and A. G. Evans, "the interfacial fracture resistance in brittle matrix composites" to be published in J. Am. Ceram. Soc.
14. A. G. Evans and J. W. Hutchinson, "Effects of non-planarity of the mixed mode fracture resistance of bimaterial interfaces", to be published in Acta metall.
15. W. Mader and M. Rühle, "Electron microscopy studies of defects at diffusion-bonded Nb/Al_2O_3 interfaces", to be published in Acta metall.
16. H. Jensen, J. W. Hutchinson and K. S. Kim, work in progress on decohesion in the cut test.
17. M-Y. He and J. W. Hutchinson, "Crack deflection at an interface between dissimilar elastic materials", to be published in Int. J. Solids Struct.

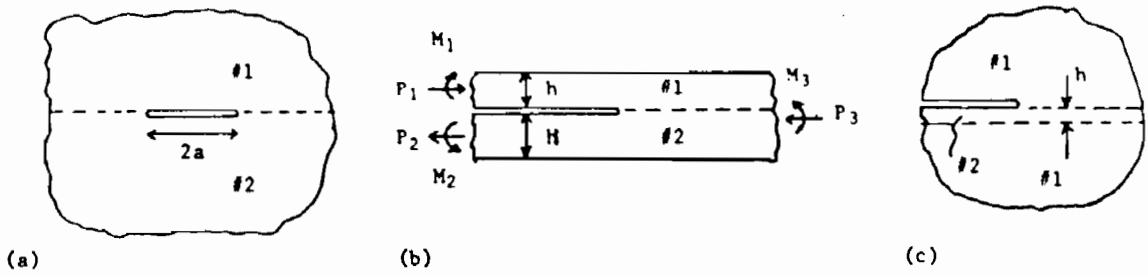

Fig. 1 Three basic interface crack geometries.

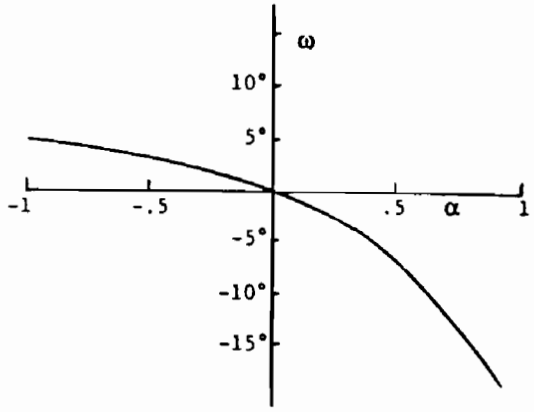

Fig. 2 Phase shift ω between remote and near-tip stress intensity factors ($\beta = 0$).

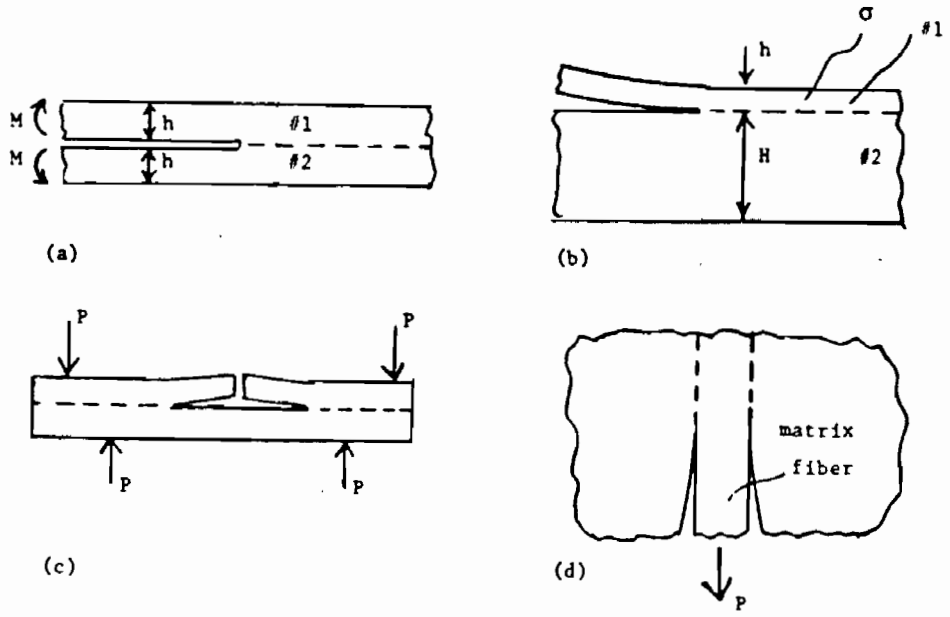

Fig. 3 Four examples illustrating range of mixed-mode conditions at the tip of an interface crack: (a) double cantilever, (b) decohesion of thin film under residual biaxial tensile stress, (c) four-point bend specimen, and (d) fiber pull-out.

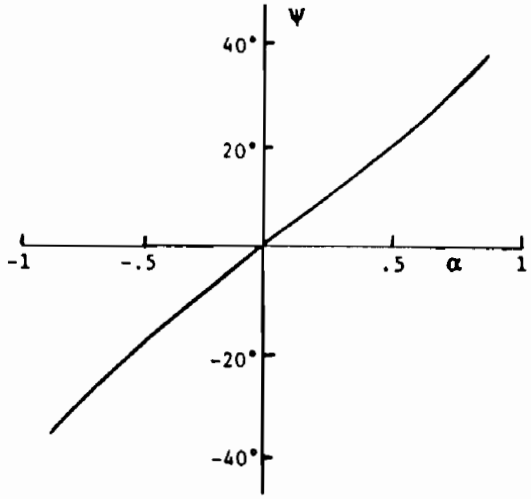

Fig. 4 Phase of stress intensities, $\psi = \tan^{-1}(K_2/K_1)$, for double cantilever in Fig. 3a (β=0).

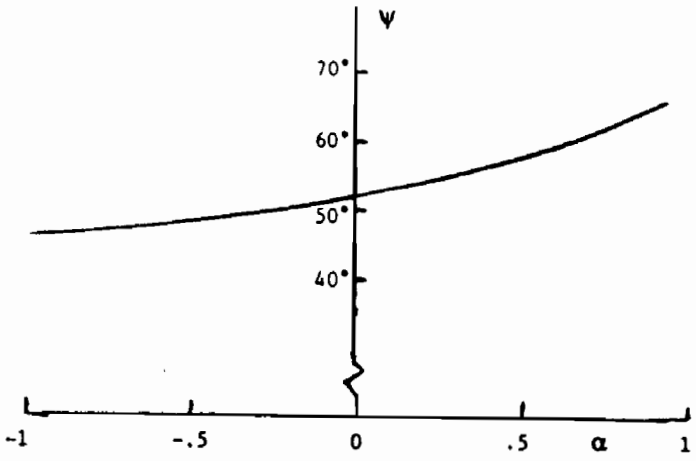

Fig. 5 Phase of stress intensities, $\psi = \tan^{-1}(K_2/K_1)$, for decohesion of thin film in Fig. 3b (β=0).

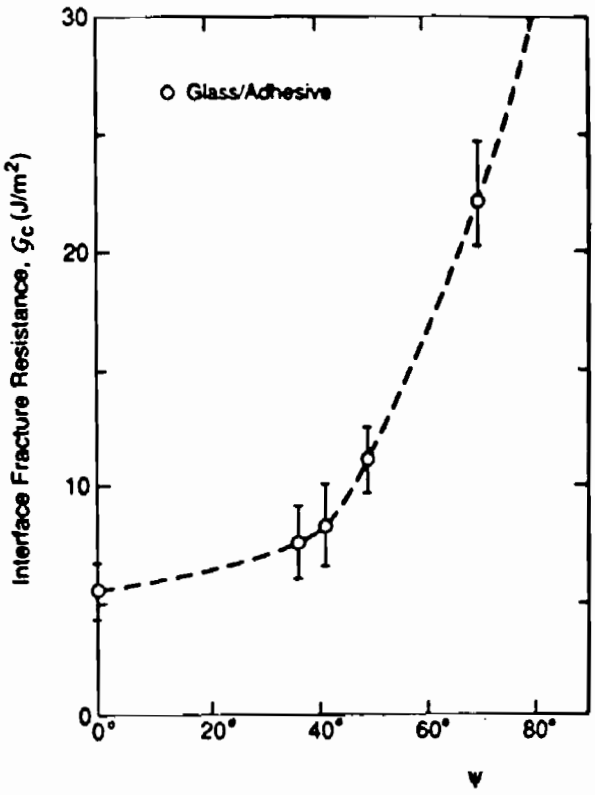

Fig. 6 Interface toughness data for an epoxy/glass system from (12).

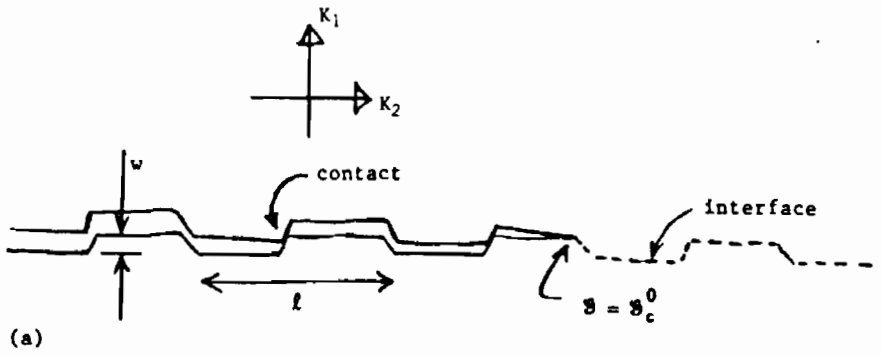

(a)

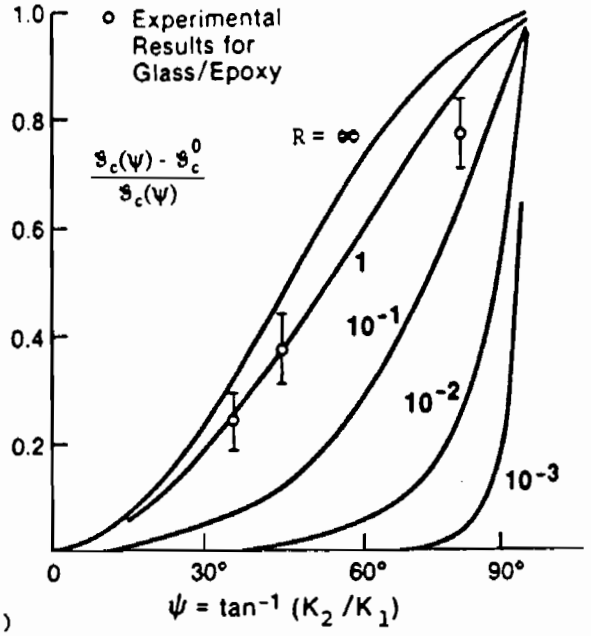

(b)

Fig. 7 Micro-mechanical model of effect of interface roughness on mixed-mode toughness.

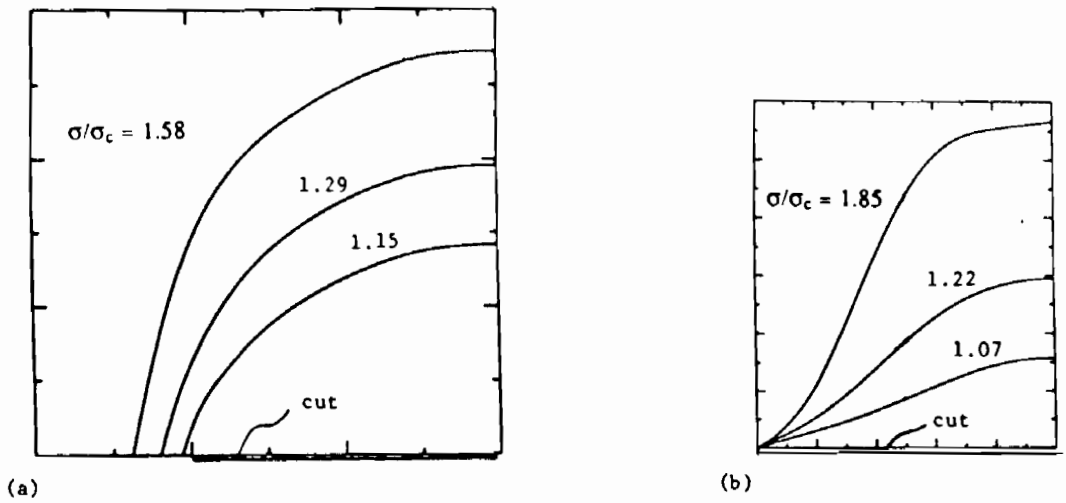

Fig. 8 Shapes of decohesion region in the cut test at various levels of σ/σ_c ($\nu_1 = 1/3$): (a) based on criterion for an ideally brittle interface, $\mathcal{G} = \mathcal{G}_c^0$; (b) based on the criterion $K_1 = K_1^c$ independent of K_2 and K_3.

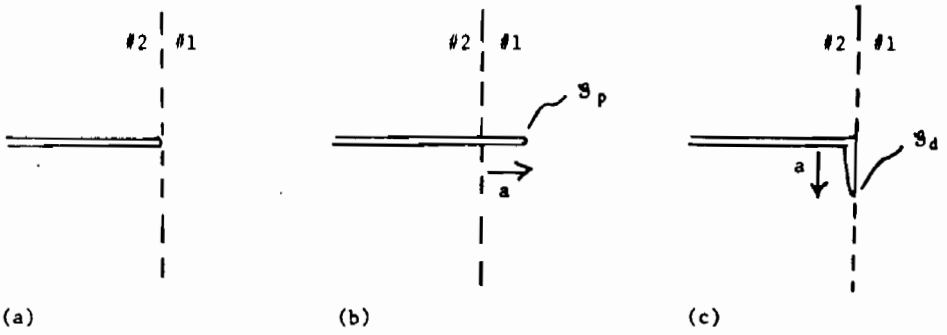

Fig. 9 Competition between crack penetration and deflection at an interface: (a) main crack at interface, (b) penetration of interface, and (c) deflection by interface.

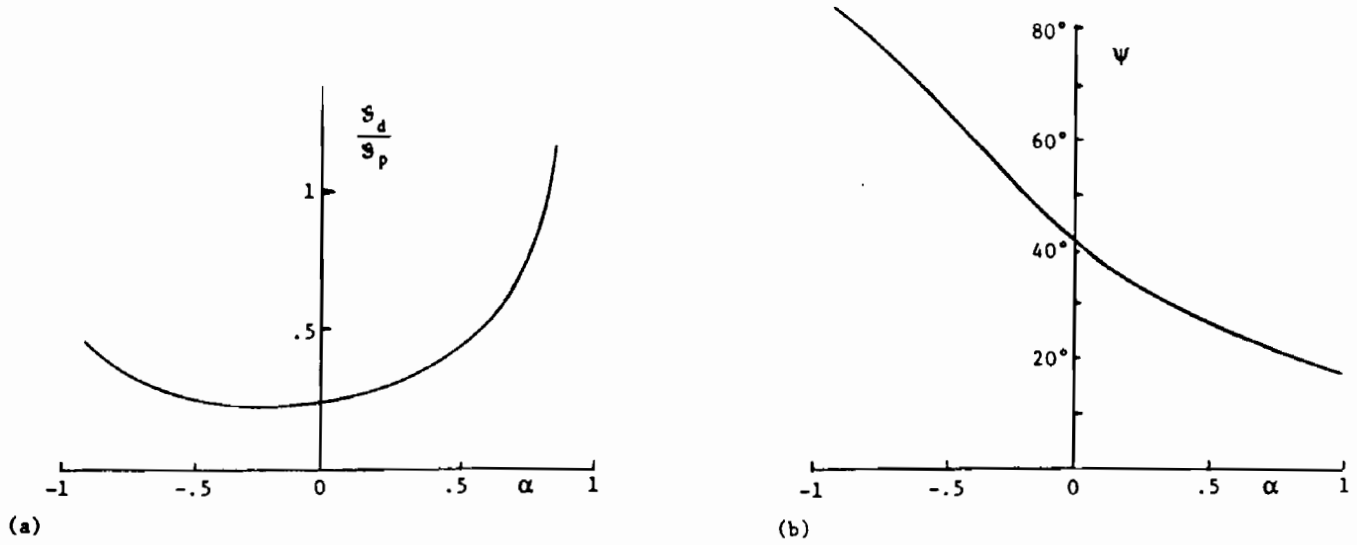

Fig. 10 (a) Ratio of energy release rate of deflected crack to that of penetrating crack as a function of the elastic mismatch parameter α (β=0). (b) Phase of stress intensities, $\psi = \tan^{-1}(K_2/K_1)$, for deflected crack tip (β=0).